Imaging and Information Processing of Pitting-Corroded Aluminum Alloy Panels with Surface Metrology Methods

Honglei Li[1], Margaret R. Garvan [2], Jiaming Li[3], Javier Echauz[4], Douglas Brown [5], George J. Vachtsevanos[6]

[1, 2, 3, 6] *Department of Electrical and Computer Engineering, Georgia Institute of Technology, Atlanta, GA, 30332, USA*

honglei.li@gatech.edu
mgarvan3@gatech.edu
jli339@gatech.edu
gjv@ece.gatech.edu

[4] *JE Research, Inc., 170 Wentworth Terrace, Alpharetta, GA 30022, USA*

echauz@ieee.org

[5] *Analatom, Inc.,562 E. Weddell Dr. Suite 4, Sunnyvale, CA 94089-2108, USA*

Doug.Brown@analatom.com

ABSTRACT

It has been established that corrosion is one of the most important factors causing structural deterioration, loss of metal, and ultimately decrease of product performance and reliability. Corrosion monitoring, accurate detection and interpretation are recognized as key enabling technologies to reduce the impact of corrosion on the integrity of critical aircraft and industrial assets. Interest in corrosion measurement covers a broad spectrum of technical approaches including acoustic, electrical and chemical methods. Surface metrology is an alternative approach used to measure corrosive rate and material loss by obtaining surface topography measurement at micrometer levels. This paper reports results from an experimental investigation of pitting corrosion detection and interpretation on aluminum alloy panels using 3D surface metrology methods, image processing and data mining techniques. Sample panels of AA 7075-T6, an aluminum alloy commonly used in aircraft structures, were coated on one side with a corrosion-protection coating and assembled in a lap-joint configuration. Then, a series of accelerated corrosion testing of the lap-joint panels were performed in a cyclic corrosion chamber running ASTM G85-A5 salt fog test. Panel surface characterization was evaluated with laser microscopy and stylus-based profilometry to obtain global and local surface images/characterization. Promising imaging and surface features were extracted and compared between the uncoated and coated panel sides, as well as on the uncoated sides under different corrosion exposure times. In the evaluation process, image processing, information processing and other data mining techniques were utilized. Information processing involves the steps of feature or Condition Indicator extraction and selection. The latter step addresses the problem of selecting those features that are maximally correlated with the actual corrosion state, for the purpose of corrosion detection, localization, quantification and state estimation. The results, verified by mass loss data, confirmed the contention that pits at the panel surfaces formed as a result of electrochemical corrosion attack, and showed that deteriorating pitting corrosion attack correlates with increasing corrosion exposure times. This study is a first step in the process of understanding, assessing and responding to the pitting corrosion and ultimately preventing material failure to insure aircraft structural integrity.

1. INTRODUCTION

Every year, corrosion is responsible for billions of dollars loss in structural deterioration, loss of metal, and ultimately decreased product performance and reliability. Pitting corrosion is one of the most prevalent forms of localized corrosion, a dangerous phenomenon because of its rapid damage growth rate, and the difficulty to detect it and predict its evolution. The pitting attack is highly localized and is usually in the form of holes that can penetrate inwards extremely rapidly and ultimately damage the structure by either perforating the material or developing into cracking due to stress corrosion (Rao & Rao, 2004). It is thus essential to insure the critical assets' integrity and operational safety by condition-based monitoring, early

detection, interpretation and prediction of pitting attack. Many research efforts have been reported in the past addressing this critical issue (Frankel, 1998; Szklarska-Smialowska, 1999; Huang & Frankel, 2006; Pereira, Silva, Acciari, Codaro & Hein, 2012). However, undeniably, well-recognized global corrosion measurements, such as weight loss and wall thickness reduction, cannot offer an appropriate and trustworthy way to interpret the pitting corrosion due to its localized attack nature. To address the need for accurate detection, interpretation and prediction of pitting corrosion, this paper proposes the use of surface metrology methods together with image and information processing techniques that take advantage of accurate and thorough testing evidence.

1.1. Motivation

Detection, localization and quantification of corrosion in complex structures over large, partially accessible areas are of growing interest in the aerospace industries. Traditionally, conventional ultrasonics and eddy current techniques have been used to precisely measure the thickness reduction in aircraft structures. However, the scanning may become impossible when the area of inspection is inaccessible. Upon this need, there has been a number of undergoing research using guided wave tomography technique to screen large areas of complex structure for corrosion detection, localization (Clarke, 2009) and defect depth mapping (Belanger, Cawley & Simonetti, 2010). However, due to the nature of ultrasonic guided wave, this technique is vulnerable to environmental changes, especially to temperature variation and surface wetness occurrence (Li, Michaels, Lee, & Michaels, 2012), and the precision of corrosion defect depth reconstruction is restricted by sensor network layout, structure complexity, and other factors, which limits the scope of the field application.

On the other hand, in the field of surface metrology, there are various techniques for quantitative characterization of surface topology, generally categorized into contact and non-contact measuring methods, which are promising techniques for corrosion, especially localized corrosion detection and characterization. The traditional contact profilometry has the merits of reliable measurement and low cost, and the disadvantage of low speed, and resolution and applicable surface limitation. On the contrary, the optical non-destructive metrology has the merits of high speed, high profiling resolution and non-destructiveness, and the disadvantage of high scatter noise and high cost.

1.2. Methodology

In this paper, we take advantage of both contact and non-contact surface metrology techniques to obtain 2D and 3D images/profiles for accurate characterization of pitting corrosion attack in AA7075-T6 aluminum alloy panels; extract and select promising morphologic and texture features from images, as well as profile features from surface measurements. Note that both global and local metrology measurements and image/profile data analysis approaches are adopted here for the purpose of accurate detection, localization and interpretation of pitting corrosion. To facilitate early detection of corrosion attack, initial testing procedures, data acquisition and feature extraction focus on global approaches, i.e., the whole panel area is viewed as the target for data collection and analysis. After the corrosion detection, localized studies are adopted where imaging studies, for example, focus on small areas of the global image where corrosion initiation is suspected, localized, or prone to spread more rapidly than other areas. The highlight of this work is the utilization of 3D surface metrology testing tools and novel image/information processing methods to study the features of interest for corrosion analysis.

The remainder of the paper is organized as follows. Section 2 introduces the procedures of accelerated corrosion testing. Section 3 describes the facilities and procedures of 3D surface metrology testing for imaging/ characterization data acquisition. Section 4 introduces the methodologies used in corrosion data mining, including image pre-processing, feature extraction and feature selection. Section 5 presents the analysis results for pitting corrosion detection, localization and interpretation. Section 6 concludes the paper with a summary of future work.

2. ACCELERATED CORROSION TESTING

2.1. Testing Preparation

New aluminum alloy AA7075-T6 and AA2024-T3 samples were cut to dimension of 6'×3'×1' and uniquely marked with stencil stamps close to the edge of both faces of the sample. A sample panel is shown in Figure 1. The samples were then cleaned using an alkaline cleaner, TURCO 4215 NC-LT – 50 g/L for 35 min at 65℃. Afterwards, the samples were rinsed with Type IV reagent grade deionized water and immersed in a solution of 20% (v/v) nitric acid for 15 minutes. The samples were then rinsed again in the deionized water and air dried. The weights were recorded to the nearest fifth significant figure and the samples were stored in a desiccator. After massing, the samples were assembled in a lap-joint configuration as shown in Figure 2, and coated with 2 mils of epoxy-based primer and 2 mils of polyurethane.
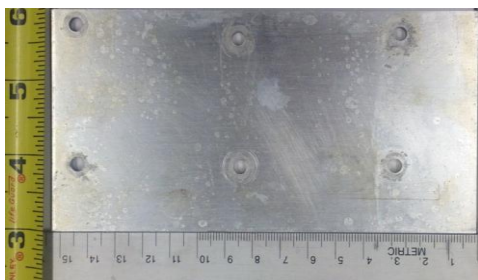
Figure 1. Corrosion panel sample on the uncoated side with 6 through rivet holes, AA 7075-T6.

Figure 2. AA7075-T6 and AA2024-T3 lap joint assembly.

2.2. Cyclic Corrosion Testing

Corrosion tests were performed in a cyclic corrosion chamber running a modified B117 salt-fog test, specifically, the ASTM G85-A5 test. This test consisted of two one hour steps. The first step involved exposing the samples to a salt fog for a period of one hour at 25 ℃. The electrolyte solution composing the fog was 0.05% sodium chloride and 0.35% ammonium sulfate in deionized water. This step was followed by a dry-off step, where the fog was purged from the chamber while the internal environment was heated to 35 ℃. Electrical connections for the flex sensors were made to an AN110 positioned outside the sealed chamber by passing extension cables through the bulkhead in the chamber. Temperature and relative humidity were acquired at 1-minute intervals.

At the conclusion of this experiment, lap joints were removed from the environmental chamber and disassembled. Following disassembly, the polyurethane and epoxy coatings on the aluminum panels were removed by placing them in a solution containing methyl ethyl ketone. After a 30-minute immersion the panels were removed and rinsed with deionized water. These panels were again alkaline cleaned with a 35-minute immersion into a constantly stirred solution of 50 g/l Turco 4215 NC-LT at 65 ℃. This was followed by a deionized water rinse and immersion into a 90 ℃ solution of 85% phosphoric acid containing 400 g/l chromium trioxide for 10 minutes. Following phosphoric acid treatment, the panels were rinsed with deionized water and placed into a 20% nitric acid solution for 5 minutes at 25 ℃. Plates were then rinsed with deionized water, dipped

in ethanol, and dried with a heat gun. This cleaning process was repeated until mass values for the panels stabilized. These values were then compared with values predicted from the results from surface metrology image processing.

This experiment ran over a period of 286 hours, where the environment inside the chamber was varied in temperature and humidity to promote corrosion. Panels 1-3 were removed 133, 209 and 286 hours from the experiment, respectively, preparing for the surface metrology testing. Detailed explanation of the accelerated corrosion testing is introduced in a complementary paper.

3. 3D SURFACE METROLOGY FOR CORROSION ANALYSIS

Surface metrology is the measurement of small-scale features on surfaces, which can be realized through contact or non-contact instruments as introduced before. Here, we utilize state-of-the-art laser microscopy and stylus-based profilometry surface measurement equipment to obtain 2D and 3D images and characterization data of corroded surfaces and extract from them relevant information that assists in corrosion detection and interpretation.

In this preliminary work, for the illustration of methodology, our study focuses on the corrosion behavior of AA 7075-T6 panels of 3 different corrosion exposure times. AA2024-T3 panels from the corresponding lap joints will be examined in the future work. In this testing, we use a confocal laser microscope and a stylus-based profilometer together to achieve a thorough examination of the corroded panels with rivet holes. The Olympus LEXT OLS4000 3D Laser Confocal Microscope, as shown in Figure 3(a), is designed for nanometer level imaging, 3D surface characterization and roughness measurement. Magnification ranges from 108x to 17,280x. The Bruker's Dektak 150 Stylus Profilometer, as shown in Figure 3(b), is a traditional 2D tactile profilometer. With the programmable map scan capability and the post-processing software, it allows for large area 3D topography coverage. The combination of the two surface metrology tools facilitates both localized and global characterization of a corroded panel at various resolution scales.

The surface metrology testing scheme is summarized as below:

1) Global characterization:

• The laser microscope can provide large area 2D microscopy imaging by stitching adjacent images.

• The stylus profilometer can provide large flat area (i.e., surface without rivet holes) 3D map scan imaging. A schematic of the area the profilometer covers in a 3D map scan for a typical panel is shown in Figure 4.
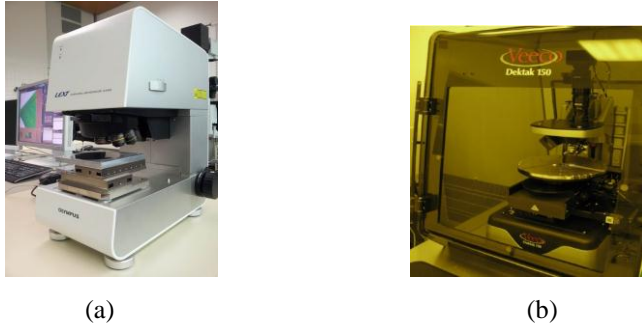
(a)   (b)

Figure 3. Surface metrology measuring tools: (a) Olympus LEXT OLS4000 3D Laser Confocal Microscope, (b) Bruker Dektak 150 Stylus Profilometer.
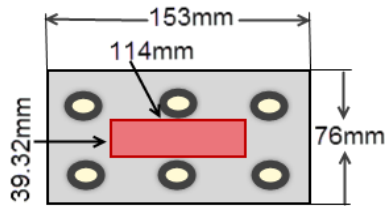

Figure 4. The area (in red) the profilometer covers in a 3D map scan.

2)   Local characterization:

• After the corrosion detection and localization, the laser microscope can provide a close look at the 3D topography of the analyzed surface areas.

First, for corrosion detection and quantification, global characterization was performed through both the microscope and the profilometer for each panel corresponding to a specific corrosion exposure time: while the microscope provided whole-panel 2D imaging, the stylus profilometer provided contact 3D map scan of the general central region without rivet holes. Next, local 3D characterization of areas of interest was conducted through the microscope. The further surface analysis was performed based on the local 3D characterization and a list of surface parameters was calculated for further processing.

4. CORROSION DATA MINING

An important and essential component of the corrosion detection and interpretation architecture involves image/characterization data pre-processing and data mining aimed to extract and select useful and relevant information from raw data. In the proposed architecture, the most important components supporting the implementation of the framework are feature extraction and selection. Features are the foundation for the fault/corrosion detection and interpretation scheme. Feature extraction and selection processes are optimized to extract only the information that is maximally correlated with the actual corrosion state. Appropriate performance metrics, such as correlation

coefficients, Fisher's Discriminant Ratio (FDR), et al. can be utilized to assist in the selection and validation processes. Figure 5 shows the overall data mining scheme. Image pre-processing, feature extraction and selection are highlighted leading to their utility in pitting corrosion detection, localization, interpretation, and eventually prediction of corrosion states.
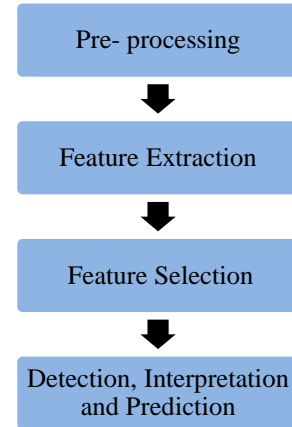

Figure 5. Corrosion data mining scheme.

4.1. Image Pre-processing

Image/data pre-processing involves filtering and preparing the data for further processing. Figure 6 shows a typical sequence of pre-processing steps of corrosion images from surface metrology testing. In the first step, de-noising, discrete stationary wavelet transform (SWT) is applied, and then histogram equalization is performed for contrast enhancement followed by applying a threshold to identify the regions of interest in the image. In this framework, image processing techniques are utilized to pre-process the global panel images as well as the local pitting area images, in preparation for the feature extraction step introduced in Section 4.2. First, globally, for each panel, successive 2D microscopic images were taken and stitched together to obtain the entire panel image. In the whole panel image pre-processing, the rivet-hole areas and artifacts (e.g., stencil-stamp marked numbers) were manually whitened so they would not be confused with corroded regions. Then, in order to identify the pitting corrosion attacked areas, a 2D median filter was applied followed by thresholding (with a threshold of 0.2) to obtain at a binary image. Second, locally, each suspected pitting area was identified from the whole panel image, and a closer microscopy examination was conducted. An example of a local pit identification process is as shown in Figure 7. To identify the pit(s) from the background, the area of each object (i.e., a black region representing a corroded region) in the binary image was calculated. The sum of objects with the area larger than 50 pixels was defined as the total area of the pitting corroded regions. Note that the identification threshold of 50 pixels was set to avoid mistaking dark regions caused by the grain boundaries as pits.

Imaging de-noising using Discrete SWT   Contrast enhancement   Thresholding
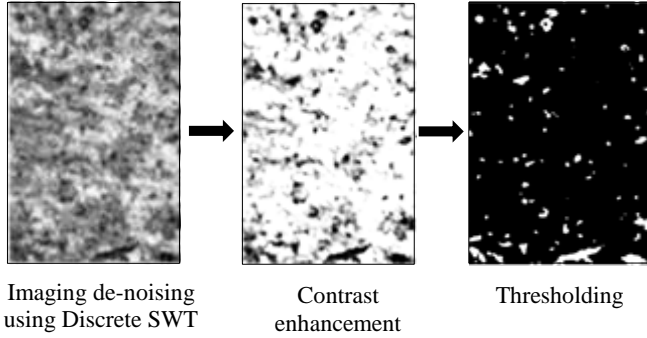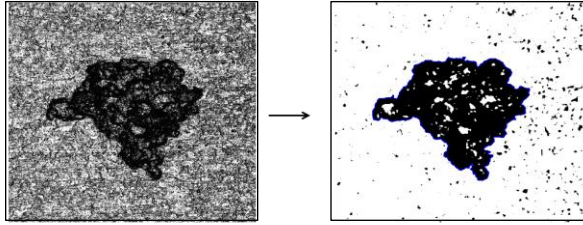
Figure 7. Local pit identification via image processing. Left: Original localized pit image; Right: Pit identified from the

background with the pit edge (in blue) identified by image processing algorithm.

4.2. Feature Extraction

There are several characterization features to quantify the pitting corrosion attack, e.g. corroded area percentage, average pit depth measurement, maximum pit depth measurement, pitting density (pits/mm^2), and remaining wall thickness due to pitting. In addition, image processing techniques can be used to extract morphological and texture features to facilitate pitting corrosion interpretation. The following outlines the features extracted from 2D corrosion images and 3D characterization data, which may facilitate the corrosion detection and interpretation:

1) Corroded Area Percentage

The pitting corroded area percentage is calculated as

$$percent\ area = 100\% \cdot \left(\frac{A_c}{A_I - A_R}\right) \qquad (1)$$

where A_c is the area of the corroded region, A_I is the area of the image and A_R is the area of the rivets.

2) Imaging Texture Features using Gray Level Co-occurrence Matrix

2D imaging texture features such as contrast, correlation, energy and homogeneity, as expressed in Eqs. (2-5), are calculated using the normalized gray level co-occurrence matrix (GLCM) denoted as p(i, j). The (i, j) value of the GLCM of an image I has the value of how often a pixel with value i occurs horizontally adjacent to a pixel with value j in image I. The contrast as in Eq. (2) returns a measure of the

intensity contrast between a pixel and its neighbor over the whole image. For a constant image, the contrast is 0. The correlation as in Eq. (3) returns a measure ranging between -1 and 1 represents how correlated a pixel is to its neighbor over the whole image. The energy as in Eq. (4) is calculated as the sum of the squared elements in the GLCM. For a constant image, the energy is 1. The homogeneity as in Eq. (5) is a measure of the closeness of the distribution of elements in the GLCM to the GLCM diagonal.

$$contrast = \sum_{i,j}|i - j|^2 p(i,j) \qquad (2)$$

$$correlation = \sum_{i,j} \frac{(i-\mu_i)(j-\mu_j)p(i,j)}{\sigma_i \sigma_j} \qquad (3)$$

$$energy = \sum_{i,j} p(i,j)^2 \qquad (4)$$

$$homogeniety = \sum_{i,j} \frac{p(i,j)}{1+|i-j|} \qquad (5)$$

3) Morphological Features

Morphological features can be extracted from 2D pitting images to characterize the shape of the pitting attacked surface area. Features such as roundness, solidity, eccentricity, major axis length and minor axis length are calculated as expressed in Eqs. (6-10):

$$roundness = \frac{4\pi A}{p^2} \qquad (6)$$

where A is the area of the region and p is the perimeter of the region.

$$solidity = \frac{Area}{ConvexArea} \qquad (7)$$

where ConvexArea is the area of the convex hull of the region.

For an ellipse defined by $\frac{x^2}{a^2} + \frac{y^2}{b^2} = 1$, the eccentricity, major axis length and minor axis length are calculated as

$$eccentricity = \sqrt{1 - \frac{b^2}{a^2}} \qquad (8)$$

$$L_{Major} = \max(2a, 2b) \qquad (9)$$

$$L_{Minor} = \min(2a, 2b). \qquad (10)$$

4) Surface Roughness

Surface roughness is a measure of the texture of a surface. It is quantified by the vertical deviations Z(x,y) of a real surface from its ideal form. If these deviations are large, the surface is rough; if they are small the surface is smooth. Roughness is typically considered to be the high frequency, short wavelength component of a measured surface. The 3D surface roughness features are listed in Table 1.

Table 1. Surface roughness parameters and their expressions.

Name	Symbol	Equation
Maximum Height	S_Z	$S_Z = S_P + S_V$
Maximum Peak Height	S_P	$S_p = \max(Z(x,y))$
Maximum Valley Depth	S_v	$S_V = \min(Z(x,y))$
Arithmetic Mean Height	S_a	$S_a = \dfrac{1}{A}\iint |Z(x,y)|dxdy$
Root Mean Squared Height	S_q	$S_q = \sqrt{\dfrac{1}{A}\iint |Z(x,y)|^2 dxdy}$
Skewness	S_{sk}	$S_{sk} = \dfrac{1}{S_q^3}\dfrac{1}{A}\iint Z(x,y)^3 dxdy$
Kurtosis	S_{ku}	$S_{ku} = \dfrac{1}{S_q^4}\dfrac{1}{A}\iint |Z(x,y)|^4 dxdy$

5) Other Characterization Features

Other pit characterization features include the corroded area geometric features (e.g., surface area, circumference), 2D pit profile (line) features (e.g., pit width, pit depth, pit profile cross-sectional area), 3D pit profile features (e.g., pit volume), et al.

4.3. Feature Selection via Performance Metrics

After a sufficient number of image/characterization features are extracted, feature selection can be conducted to determine the smallest subset of features that satisfies given performance criteria. Performance metrics such as correlation coefficient and Fisher discriminant ratio (FDR) can be applied to assess the feature quality. Optimization and Principle Component Analysis (PCA) tools can be used for this purpose. Then a list of "best" features can be selected based on the feature performance. Here we use correlation coefficient and FDR to gauge the image features:

1) Correlation Coefficient

The correlation coefficient is defined as

$$\rho_{X,Y} = \frac{E[(X-\mu_X)(Y-\mu_Y)]}{\sigma_X \sigma_Y} \qquad (11)$$

where, X and Y are two random variables with expected values μ_X and μ_Y and standard deviations σ_X and σ_Y. The estimate of the correlation coefficient can be expressed as

$$r_{xy} = \frac{\sum(x_i-\bar{x})(y_i-\bar{y})}{\sum(x_i-\bar{x})^2 \sum(y_i-\bar{y})^2} \qquad (12)$$

where $\bar{x}$ and $\bar{y}$ are the sample means of X and Y.

2) Fisher Discriminant Ratio (FDR)

Fisher's linear discriminant is a classification method that projects high-dimensional data onto a line and performs classification in this one-dimensional space. The projection maximizes the distance between the means of the two classes while minimizing the variance within each class. This defines the Fisher criterion, or FDR, which is maximized over all linear projections. The FDR of two classes is given as

$$FDR = \frac{(\mu_1-\mu_2)^2}{\sigma_1^2+\sigma_2^2} \qquad (13)$$

where μ represents a mean, σ represents a variance, and the subscripts denote the two classes.

5. RESULTS AND DISCUSSION

In this paper, we assume that in the accelerated corrosion testing, the corrosion protection coating prevents the corrosion attack up to the maximum hours of corrosion exposure (i.e., 286 hours), and thus we use the measurement from panel coated sides as "baselines", and compare to the one from the panel uncoated sides.

5.1 Corrosion Characterization Features

Preliminary global inspection through the profilometer 3D map scan indicated that the corroded panels were pretty flat without noticeable low-frequency surface irregularities, and thus the surface features can be mostly captured by roughness. Therefore, we can omit waviness for this application. Thus, smoothness and spike removal filters were generally applied at the raw profile measurement from the profilometer and the microscope. Figure 8 (a) and (b) provide the 2D microscopic images of the local pitted panel areas of the same size and magnification in Panel 1 and 2, and Figure 8 (c) and (d) illustrate typical pit cross-sectional profiles from Panel 1 and 2 respectively, with (d) corresponding to the colored line marked in (b). Figure 9 shows a 3D topology image of an area of connected pitting in Panel 2. Table 2 lists the 2D pit profile measurement of the colored lines in Figure 8 (b) and Figure 9, of which the pit height represents the maximum pit depth.

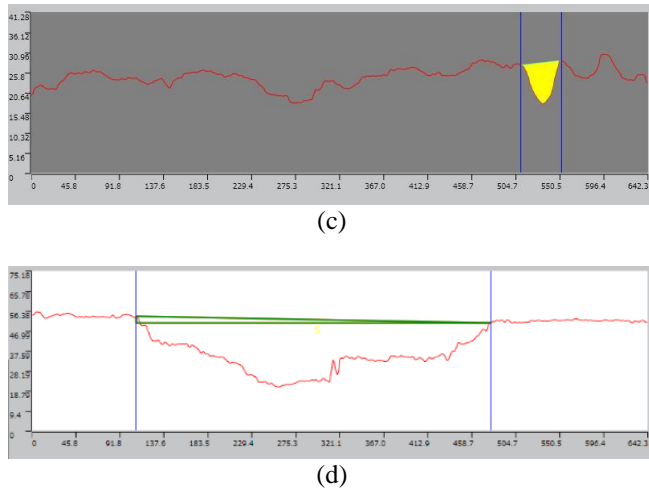(a)   (b)

(c)

(d)
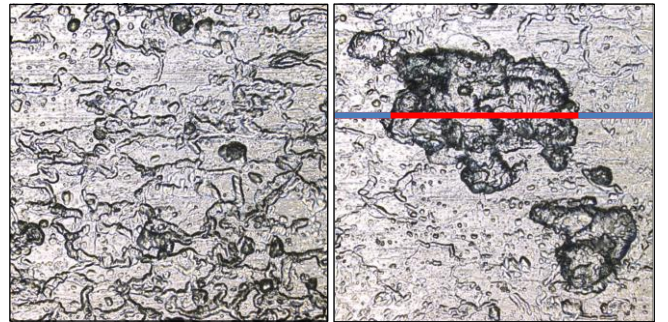
Figure 8. 2D characterization of pitted panel areas (642 × 644 μm^2) on the uncoated side of (a) Panel 1, and (b) Panel 2; pit cross-sectional profile measurement (in μm) of (c) a general pit in Panel 1 (with the highlighted cross-sectional area of 240.43 μm^2), and (d) the colored line in (b), Panel 2.
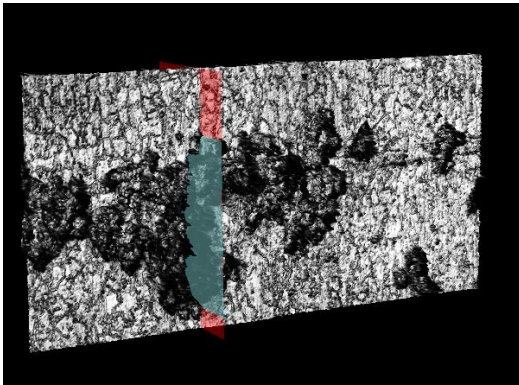

Figure 9. 3D characterization of a pitted panel area (2561 × 1278 μm^2) on the uncoated side of Panel 2, with the corresponding cross-sectional profile measurement as listed in Table 2.

Table 2. Corresponding 2D pit profile measurement (in μm) of the colored lines in Figure 8(b) and Figure 9, Panel 2.

Measurement	Figure 8 (b)	Figure 9
Width (μm)	369.432	848.483
Height(μm)	3.164	19.895
Length(μm)	369.445	848.717

Except for the 2D pit profile features such as pit width and pit depth, geometric features such as pitting surface area and circumference (as shown in Figure 11 and Table 4) and pit volume (as shown in Figure 10 and Table 3) can also provide solid measures for local pitting severity, of which pit volume is of importance, due to the irregular growth pattern of pitting corrosion. In Figure 10 and Figure 11, a surface height threshold was manually chosen respectively, in order to calculate the corroded surface area and the

underneath pitting volume. In Figure 11, as calculated from Table 4, the pitting affected surface area was in total of 258,380.787 μm^2, or 3.94% of the entire examined surface area.

Detailed analysis of the above pitting characterization results revealed some interesting findings. First, morphological analysis of the pits in Panel 1 and Panel 2 indicated that, the nucleated pits, as those general non-visible ones in Panel 1, usually took regular morphological forms, such as hemi-spherical, near-hemispherical and near-conical shapes as indicated in Figure 8 (a) and (c). As the corrosion exposure time increased, a few nucleated pits evolved into irregular shapes with the pit dimension increased, as indicated in Figure 8 (b) and (d). From a side-by-side comparison in Figure 8 (a) and (b), it is noted that, in Panel 2, even though some nucleated pits evolved into bigger and irregular pits, the majority of the pit population were still in a regular shape with similar dimensions as the nucleated pits in Panel 1. Second, as noted from Table 2, a prevalent phenomenon among the big visible pits in Panel 2 and 3 was that, a pit's width was usually significantly larger than its depth, which suggests that the metal dissolution rate was higher at the pit wall than at the pit bottom. In summary, from localized pitting characterization analysis of all three panels, it is concluded that on Panel 1, a number of nucleated pits formed, but generally few big visible pits existed; from Panel 1 to 2, as the corrosion exposure time increased from 133 hours to 209 hours, there emerged a few visible pits assuming irregular shapes, very likely with a much bigger width than depth; from Panel 2 to 3, as exposure time further increased to 286 hours, more and more large visible pits formed, located most likely close to panel edges, rivet hole edges and surface irregularies. Note that, due to the nature of the accelerated corrosion testing, three panels, instead of one, were exposed to three different corrosion emersion times respectively. Thus, an individual pit characterization growth cannot be observed in this study. Instead, 3D microscopic characterization studies of a number of random pits were conducted in each panel. It is indicated from the results of the three panels that, even though there was a big scatter of the characterization data of the visible pits on Panel 2 and 3, the number of big visible pits and the connected pitting areas increased with exposure time.
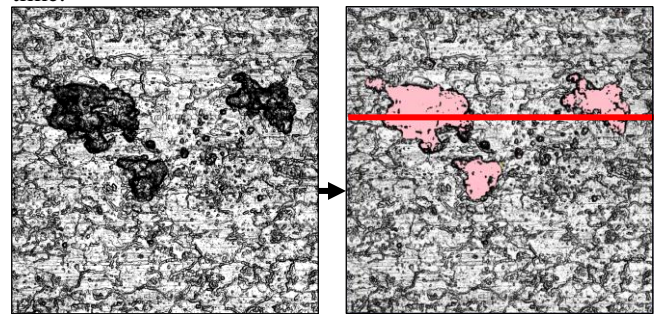

Figure 10. Surface height thresholding procedure to obtain the 3D pitting characterization as shown in Table 3 for a

pitted panel area (1278 $\times$ 1281 μm^2) on the uncoated side of Panel 2.

Table 3. Corresponding 3D pitting characterization measurement of the area in Figure 10.

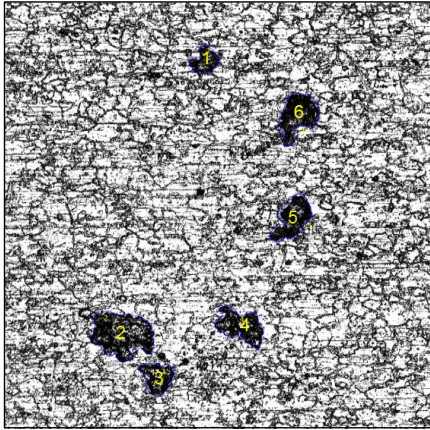| Cross-sectional Area(μm^2) (of the red line in Figure 10)	103,366.090
Surface Area (μm^2)	192,043.495
Volume (μm^3)	1,101,417.185

Figure 11. Pitted panel area (2553 $\times$ 2568 μm^2) on the uncoated side of Panel 2, with the corresponding 6-pit geometric measurement as listed in Table 4.

Table 4. Corresponding 3D pitting characterization measurement of the area in Figure 11.

No.	Surface Area(μm^2)	Circumference (μm)
1	20,081.765	679.027
2	79,576.806	1,333.879
3	28,428.326	770.822
4	43,645.952	1,216.175
5	39,969.714	1,053.796
6	46,678.224	1,110.563

5.2 Corrosion Image Features

5.2.1 Image Pre-processing

In addition to local pitting characterization analysis, 2D panel images were acquired successively and pre-processed in preparation for corrosion image feature extraction. For each panel, 2D microscopic images of size 37 x 37 mm were taken using LEXT OLS4000 with a magnification setting of 108x, and then stitched together to obtain the entire panel image. Figure 12 depicts the stitched whole panel microscopic images of Panel 1, 2 and 3 and their corresponding binary images after image pre-processing.
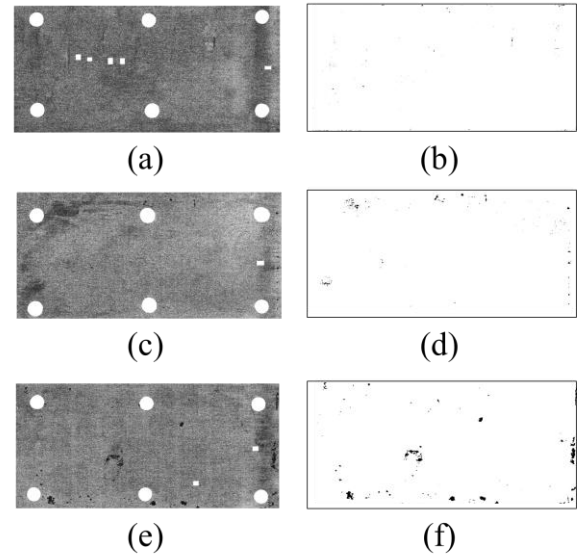

Figure 12. Whole panel image pre-processing. Left column: intermediary images with rivet holes and marked numbers whitened of (a) Panel 1 with 133-hr corrosion exposure, (c) Panel 2 with 209-hr corrosion exposure, (e) Panel 3 with 286-hr corrosion exposure. Right column: binary images after pre-processing of (b) Panel 1, (d) Panel 2, (f) Panel 3.

5.2.2 Feature Extraction, Selection and Data Mining

Features extracted from segments of the corrosion images can be used to classify the state of corrosion in the corresponding image segment. Figure 13 shows an example set of corrosion images used for feature extraction. The top row is a set of 8 low corrosion images and the bottom row is a set of 8 high corrosion images. Contrast, correlation, energy and homogeneity features of the example corrosion images in Figure 13 were calculated and illustrated in Figure 14. The corresponding feature performance was evaluated using FDR as listed in **Table 5**. Table 5 indicates that correlation, energy and homogeneity are good image features for corrosion detection and corrosion state classification, whereas contrast performs poorly.
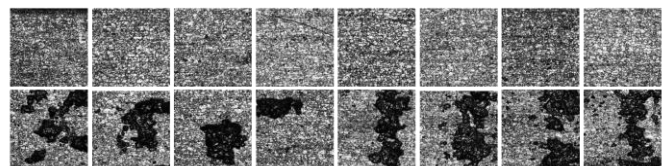

Figure 13. Example corrosion images. Top row: low corrosion. Bottom row: high corrosion.
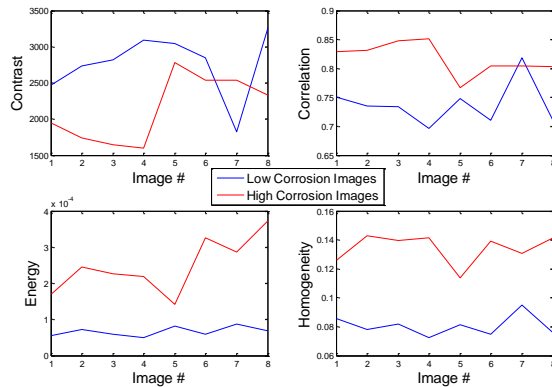
Figure 14. Contrast, Correlation, Energy and Homogeneity features of low and high corrosion images from Figure 13 (image number ascends correspond to the sequence from left to right in each row of Figure 13).

Table 5. FDR values of image features.

Features	Contrast	Correlation	Energy	Homogeneity
FDR	0.9604	2.2084	95.1962	27.3738

Figure 15 shows the corroded area percentage of the panels that had corrosion exposure times of 133, 209 and 286 hours. The resulting corroded area percentage feature was highly correlated with the measured panel mass loss as shown in Figure 15. The correlation coefficient r_{xy} of the corroded area percentage and the corresponding measured panel mass loss is 0.9727.
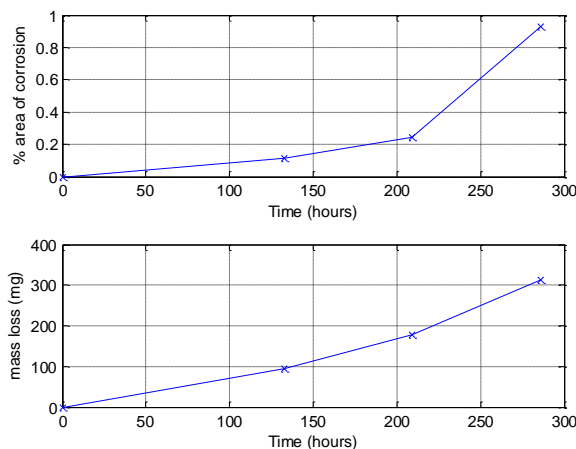

Figure 15. Top: Corroded area percentage over time. Bottom: Measured mass loss (mg) over time.

6. CONCLUSIONS

This paper reports results from an experimental investigation of pitting corrosion detection and interpretation on aluminum alloy panels using surface metrology methods, image processing and information processing techniques. Accelerated corrosion testing of the lap-joint panels was performed in a cyclic corrosion chamber running ASTM G85-A5 salt fog test. Then the global and local corrosion behaviors were imaged and characterized via microscopy and profilometry examination. Data mining techniques are utilized, including image pre-processing, image and characterization feature extraction and selection, to facilitate the study of corrosion morphological behavior and its progression as a function of corrosion exposure time. The morphological study showed that facing electrochemical corrosion attack, pits initiated and predominantly assumed in regular shapes, but underwent irregular thus progressive geometric transitions associated with increased corrosion exposure time. This study also examined a list of promising characterization and image features and conducted the performance evaluation of some representative features for corrosion interpretation. This study is a first step in the process of understanding, assessing and responding to the pitting corrosion and ultimately preventing material failure to insure aircraft structural integrity. Future work may include more rigorous testing and analysis methods, e.g., to study an individual pit evolution over time, and the evolution from pitting to cracking under stress corrosion condition; and further in the direction of aircraft structure health management, to accurately model the corrosion progression, assess the corrosion states, and predict the corrosion-induced structure failure.

REFERENCES

Belanger, P., Cawley, P. and Simonetti, F. (2010). Guided wave diffraction tomography within the Born approximation, *IEEE Trans UFFC*, Vol. 57, pp. 1405-1418.

Clark, T., (2009). *Guided wave health monitoring of complex structures*. Doctoral dissertation. Imperial College London, London, United Kingdom.

Frankel, G. S. (1998). Pitting corrosion of metals a review of the critical factors. *Journal of the Electrochemical Society*, 145(6), 2186-2198.

Huang, T.-S. & Frankel, G. S. (2006). Influence of Grain Struc- ture on Anisotropic Localized Corrosion Kinetics of AA7xxx-T6 Alloys. *Corrosion Engineering, Science and Technology*, Vol. 41, No. 3, pp. 192-199. doi:10.1179/174327806X120739.

Li, H., Michaels, J. E., Lee, S. J., Michaels, & T. E., Thompson, D. O., & Chimenti, D. E. (2012).

Quantification of surface wetting in plate-like structures via guided waves. *In AIP Conference Proceedings-American Institute of Physics*, Vol. 1430, No. 1, p. 217.

Pereira, M. C., Silva, J. W., Acciari, H. A., Codaro, E. N., & Hein, L. R. (2012). Morphology Characterization and Kinetics Evaluation of Pitting Corrosion of Commercially Pure Aluminium by Digital Image Analysis. *Materials Sciences & Applications*, 3(5), pp. 287-293.

Rao, K. S., & Rao, K. P. (2004). Pitting Corrosion of Heat-Treatable Aluminium Alloys and Welds: A Review. *Transactions of the Indian Institute of Metals*, Vol. 57, No. 6, pp. 593-610.

Shell, E. B., Buchheit, R. G., & Zoofan, B. (2005). Correlation of residual fatigue life with quantified NDE measurements. *International Journal of Fatigue*, 27(2), 105-112.

Silva, J. W. J., Bustamante, A. G., Codaro, E. N., Nakazato, R. Z., & Hein, L. R. O. (2004). Morphological Analysis of Pits Formed on Al 2024-T3 in Chloride Aqueous Solution. *Applied Surface Science*, Vol. 236, No. 1-4, pp. 356-365. doi:10.1016/j.apsusc.2004.05.007.

Szklarska-Smialowska, Z. (1999). Pitting corrosion of aluminum. *Corrosion Science*, 41(9), 1743-1767.

Trdan, U., Ocaña, J.L., Grum, J. (2009). Surface Evaluation of Laser Shock Processed Aluminum Alloy After Pitting Corrosion Attack with Optical 3-D Metrology Method. *The 10th International Conference of the Slovenian Society for Non-Destructive Testing*, September 1-3, 2009, Ljubljana, Slovenia.

BIOGRAPHIES

Honglei Li received her masters' degree in Electrical and Computer Engineering (ECE) from the Georgia Institute of Technology, and in Instrumental Engineering from Shanghai Jiao Tong University in 2010. Prior to joining Intelligent Control Systems Laboratory (ICSL) in 2012 as a graduate research assistant, she had years of interdisciplinary research experience in Non-destructive Testing & Evaluation, and biomedical engineering fields. Currently she is also working on her doctoral degree in ECE at the Georgia Institute of Technology. Her current research interests include methodologies for Structural Health Monitoring (SHM), Prognostics & Health Management (PHM), as well as incorporating of PHM for engineered system life cycle management.

Jiaming Li received the B.S degree from the University of Science and Technology of China, in 2011, the M.S. degree from Georgia Institute of Technology, in 2014. Now he is working on his Ph.D. degree in Georgia Institute of Technology. He is currently a Graduate Research Assistant with the Department of Electrical and Computer Engineering, Georgia Institute of Technology, Atlanta. His current research interests include human-machine interface, fault diagnosis and failure prognosis.

Javier Echauz is Senior Research/Data Scientist and President of JE Research, Inc., a biomedical engineering consultancy he founded in 2008 focused on computational intelligence and devices for epilepsy. In 1995, he obtained a Ph.D. degree from Georgia Institute of Technology on intelligent controls and EEG analysis under mentorship of Dr. George Vachtsevanos at Tech, and jointly Dr. Kimford Meador at Medical College of Georgia. Dr. Echauz was a tenured Associate Professor and Associate Director of the Electrical and Computer Engineering Department at University of Puerto Rico—Mayagüez before returning to Atlanta in 2000. With the Jacoby Group support, he cofounded IntelliMedix, Inc., and later BioQuantix Corp., where algorithms and intellectual property were developed and crosslicensed in collaboration with Dr. Brian Litt at Emory and Penn. He was Senior Research Scientist at NeuroPace, Inc., responsible for the seizure detection system of an implantable brain neurostimulator for epilepsy, recenty approved by the FDA. With NeuroVista Corp., Dr. Echauz developed algorithms and data quality protocols resulting in an implantable seizure advisory system. He later developed text mining interactive web applications for drug discovery, and built an EEG system for monitoring level of consciousness during seizures and PNES. Dr. Echauz has co-authored over 60 technical papers, 5 book chapters, and 12 issued patents.

Douglas W. Brown is the Senior Systems Engineer for Analatom, Inc. He received the bachelor of science degree in electrical engineering from the Rochester Institute of Technology and his master of science and doctor of philosophy degrees in electrical engineering from the Georgia Institute of Technology. Dr. Brown has ten years of experience developing and maturing Prognostics & Health Management (PHM) and fault-tolerant control systems in avionics application. He is a recipient of the National Defense Science and Engineering Graduate (NDSEG)

Fellowship and has received several best-paper awards in his work in PHM and fault-tolerant control.

George J. Vachtsevanos is a Professor Emeritus of Electrical and Computer Engineering at the Georgia Institute of Technology. He was awarded a B.E.E. degree from the City College of New York in 1962, a M.E.E. degree from New York University in 1963 and the Ph.D. degree in Electrical Engineering from the City University of New York in 1970. He directs the Intelligent Control Systems laboratory at Georgia Tech where faculty and students are conducting research in intelligent control, neurotechnology and cardiotechnology, fault diagnosis and prognosis of large-scale dynamical systems and control technologies for Unmanned Aerial Vehicles. His work is funded by government agencies and industry. He has published over 240 technical papers and is a senior member of IEEE. Dr. Vachtsevanos was awarded the IEEE Control Systems Magazine Outstanding Paper Award for the years 2002-2003 (with L. Wills and B. Heck). He was also awarded the 2002-2003 Georgia Tech School of Electrical and Computer Engineering Distinguished Professor Award and the 2003-2004 Georgia Institute of Technology Outstanding Interdisciplinary Activities Award.